Proceedings of the Korean Nuclear Society Autumn Meeting
Seoul, Korea, October 1998

First-Principle Analyses of Gap Cooling Within the Reactor Vessel

Yong Hoon Kim, Kune Y. Suh

Seoul National University
San 56-1 Shinrim-dong, Kwanak-gu, Seoul, 151-742, Korea

Abstract

First-principle analyses were performed to determine the maximum heat removal capability from the debris through the gap that may be formed during a core melt accident. Cases studied included four different nuclear power plants (TMI-2, KORI-2 ,YGN 3&4 and KNGR) per the thermal power output. Results of the analysis showed that the heat removal through gap cooling relative to flooding was efficacious as much as about 40% of the core material accumulated in the lower plenum. The three nuclear reactor (KORI-2, YGN 3&4 and KNGR) calculation results for heat removal through the debris-to-vessel gap size of about 1mm were compared with the TMI-2 reactor calculation results for the case of gap cooling alone.

1. INTRODUCTION

A cooling mechanism due to boiling in a gap between the debris crust and the RPV wall was proposed for the TMI-2 reactor accident analysis [1, 2, 3, 4]. If there is enough heat transfer through the gap to cool the outer surface of the debris and the inner surface of the wall, the RPV wall may preserve its integrity during a severe core melt accident.

In preliminary LAVA experiments performed at the Korea Atomic Energy Research Institute (KAERI), the influence of internal pressure load on the lower head vessel wall and the materials of the simulant melt on gap formation was investigated [5]. In parallel, VISU experiments at KAERI demonstrated that the heat transfer through the gap was related to the counter-current flow limitation (CCFL) [6]. While relevant experiments are being carried out in the U.S. [7] and Japan [8] as well as in Korea to understand the baseline heat transfer mechanism through the multidimensional gap, the databank is quite limited and mechanistic predictive tools are yet to be developed.

If the heat removal through gap cooling relative to CCFL is pronounced, the safety margin of the reactor can be far greater than what had been previously known in the severe accident management arena. Should a severe accident take place, the RPV integrity will be maintained because of the inherent nature of degraded core coolability inside the lower head due to boiling in a narrow gap between the debris crust and the RPV wall. As a defense-in-depth measure, heat removal capability by gap cooling coupled with external cooling can be examined for the Korean Standard Nuclear Power Plants (KSNPP) and the Korean Next Generation Reactor (KNGR) in light of the TMI-2 vessel survival.

Until now there have been no experimental data for gap cooling in the hemispherical vessel geometry and no systematic investigation with narrow gaps, especially with the hemispherical gap geometry. For this reason, under the accident scenario similar to that of TMI-2 in which reactor core melting did occur, this paper presents the results of maximum heat removal capability in the narrow gap for nuclear power reactors with differing thermal output. The nuclear power plant adopted in this paper can be classified per the nominal operating thermal power. KORI-2, YGN 3&4 and KNGR nuclear power plants in Korea

have the thermal powers on the order of 2000 MWt, 3000 MWt and 4000 MWt, respectively.

2. THEORETICAL BACKGROUND

Since the gap size is of millimeter order, cooling mechanism through the narrow gap between the debris crust and the RPV will most likely be governed by CCFL or flooding. Therefore, it is important to identify the CCFL characteristics in the narrow gap. Previous CCFL work included studies for inlet entrance, inclined channel, gap effects, and so forth. However, the CCFL correlation applicable to the annular gap in the hemispherical geometry filled with debris is nonexistent.

2.1. CCFL Correlation for Annuli

The simultaneous flow of liquid downwards in a conduit has its limitations. The higher the gas flow rate, the lower the possible liquid flow rate. The limit of this counter-current flow is called flooding or CCFL. Experiments on this CCFL have resulted essentially in two types of correlation. Of special interest is the work done by Pushkina & Sorokin [9]. Their correlation is given below.

$$Ku_G^{1/2} + m_k Ku_L^{1/2} = C_k \quad (1)$$

where $Ku_k = j_k\left[\frac{\rho_k^2}{\sigma g(\rho_L - \rho_G)}\right]^{1/4}$, k = Gas(G), Liquid(L)

This equation is called the Kutateladze correlation. They performed experiments in various diameter tubes to evaluate the zero penetration point (no liquid down) as a function of pipe size. Their conclusion was that the gas velocity sufficient to prevent any liquid from penetrating downwards is constant and independent of the pipe size (at least for pipe diameters 0.15m and above). The other correlation describing not only the minimum gas velocity for zero liquid penetration but also delivery of liquid as a function of the gas flow rate can be taken from Wallis [10] as

$$j_G^{*1/2} + m j_L^{*1/2} = C \quad (2)$$

where $j_k^* = j_k\left[\frac{\rho_k}{Dg(\rho_L - \rho_G)}\right]^{1/2}$, k = Gas(G), Liquid(L)

This correlation, derived from experiments in small pipes, predicts the gas velocity for zero penetration to be proportional to the square root of the diameter, thus increasing with pipe size.
Equations (1) and (2) contradict each other when used in the same geometry range. The former predicts no geometric dependency of the gas flow rate for zero penetration while the latter does. However, Richter [11] presented a flooding analysis which unified the whole geometry range in one equation applicable not only for zero penetration but also for partial delivery of liquid. The nondimensional velocity j_G^* of equation (2) is related to the Kutateladze number through

$$Ku_k = j_k^* D^{*1/2} = j_k^* Bo^{1/4} \quad (3)$$

where $D^* = Bo^{1/2} = D\left[\frac{g(\rho_L - \rho_G)}{\sigma}\right]^{1/2}$

The characteristic length (D) of the nondimensional velocity in equations (2) and (3) is determined from the geometry. In the tube, annuli and rectangle geometries, the characteristic length is the diameter, average circumference of annuli and wide width, respectively.

In this study, since the flooding behavior in the annuli is of special interest, the flooding correlation in annuli of Richter [11] is introduced below.

$$C_w Bo^3 j_G^{*6} S^{*2} j_L^{*2} + C_w Bo\, j_G^{*4} + 150 C_w \frac{j_G^{*2}}{S^*} = 0 \quad (4)$$

where $S^* = \frac{S}{w}$

For zero liquid penetration, i.e. $j_L^* = 0$, equation (4) can be converted as follows.

$$j_G^{*2} = -\frac{75}{BoS^*}\left[1-\left(1+\frac{BoS^{*2}}{75^2 C_w}\right)^{1/2}\right] \quad (5)$$

If the last term in equation (5) is less than 1, the gas velocity for liquid zero penetration is given as

$$j_G^{*1/2} = 0.4 \quad (6)$$

To obtain the gas velocity for liquid zero penetration into a gap, equation (6) is consistently applied in this study.

2.2. CHF in Hemispherical Geometry

Although a great deal of studies on CHF were carried out during the last decade, an exact theory of the CHF has not yet been formulated. Since the CHF is a very complicated phenomenon, it is practically impossible to theorize an exact model capable of explaining the detailed mechanism of the CHF completely. However, there are two models that are useful in explaining the CHF phenomenon. Two such primary models of CHF have been put forward in the last decade : i.e. the hydrodynamic instability model [12] and the macrolayer dryout model [13].

Widely accepted hydrodynamic CHF models have been developed by Zuber for upward-facing surface heating. The CHF for upward-facing surface is determined by the balance between the vapor generation rate and the critical vapor escape rate. The well-known CHF correlation for the case of conventional pool boiling on upward-facing heating is given below.

$$q_{CHF} = C\rho_G H_{fg}\left\{\frac{\sigma(\rho_L-\rho_G)}{\rho_G^2}\right\} \quad (7)$$

where C=0.131 by Zuber [12]

However, the CHF mechanism for a hemispherical geometry in the present study is different from upward facing surface heating. For the downward-facing boiling on the surface of a heated hemispherical debris in this study, the buoyancy force and the surface tension force that act upon the vapor bubbles are not opposing to one another. Fig. 1 shows the conceptual sketches of the bubble behavior with differing heating methods.

Cheung [14] intended to establish a proper scaling law and develop a design correlation for prediction of the CHF on the external surface of a large hemispherical vessel. A theoretical model was developed to predict the CHF limit for a saturated pool boiling on the outer surface of a heated hemispherical vessel. The model considers the existence of a microlayer underneath an elongated vapor slug on a downward-facing curved heating surfaces. Since the thickness of the two-phase boundary laryer in the external cooling case is nearly of centimeter order, Cheung's model may not properly be applied to the cooling within the hemispherical gap cooling in the range of millimeters. In the CHF experiments for the hemispherical narrow gaps and visualization experiments in the same geometry performed at KAERI, CCFL occurred at the top end of the gap and prevented water from penetrating the gap. That is, CCFL brought about local dryout and finally, CHF in hemispherical narrow gaps [15]. When top flooding occurs in a hemispherical narrow gap, the maximum heat removal capability can be determined.

3. MAXIMUM HEAT REMOVAL CAPABILITY

3.1. Material Characteristics of Debris

In order to investigate the lower head debris behavior in the TMI-2 reactor, thermophysical properties were estimated for the debris on the lower head consisting of a solidified continuous hard layer, from which companion samples were cut, covered by a bed of loose debris. Samples of the solidified debris from the hard layer in contact with the lower head, termed companion samples, were extracted from the

vessel in order to assess the properties of the melt [16]. Densities of nine companion samples ranged from 7.45 g/cm^3 to 9.40 g/cm^3, with an average of 8.4±0.6 g/cm^3. The microstructure observed in the samples indicated an overall composition that was uranium-rich (U,Zr)O_2. Radiochemical analyses of the debris indicated that the debris was composed of about 70 $^w/_o$ U, 13.75 $^w/_o$ Zr, and 13 $^w/_o$ O. This composition accounts for about 97 $^w/_o$ of the debris. The remaining 3 $^w/_o$ represents stainless steel and Inconel constituents that were probably melted during relocation. In the TMI-2 Vessel Investigation Project Integration Report [17], decay heat calculations were performed to estimate heat generated within the hard layer of debris upon the lower head.

The material composition of the TMI-2 debris compound estimated to be of $78\ ^w/_o\ UO_2 - 17\ ^w/_o\ ZrO_2$ weight fraction [17]. In case that the material composition of fuel debris in other reactors is similar to that in the TMI-2 reactor, specific heat capacity will nearly be the same. Because most material relocated from the core to the lower head vessel had temperatures in the range of 2873K and 3123K [18], the pouring debris will be between liquid and solid phases. In the UO_2 and ZrO_2 specific heat capacity data [19], the values of UO_2 and ZrO_2 specific heat capacity in the liquid state is 0.502 kJ/kgK and 0.810 kJ/kgK, respectively. Then the specific heat capacity for a $78\ ^w/_o\ UO_2 - 17\ ^w/_o\ ZrO_2$ and $80\ ^w/_o\ UO_2 - 20\ ^w/_o\ ZrO_2$ weight fraction compound will have approximately 0.56 kJ/kgK and 0.563 kJ/kgK, respectively.

Hofmann et al. [18] indicated that a well-mixed (U,Zr)O_2 solid solution, as shown by the metallography and SEM results, would be expected to be found in a peak temperature range between 2873K and 3123K. Consequently, it was suggested that the peak temperature of the melt that relocated to the lower head was at least 2873K. Because of scarcity of data, however, cooling rate of the debris was not well known. However, Rempe et al. [20] indicated that cooling rate of the debris was 0.4 ~ 110 K/sec. In this study, a cooling rate of 1 K/sec is used. This assumption is perhaps overly conservative, though.

3.2. Maximum Heat Removal Requirement

In order to calculate the geometric structure of debris relocated after shutdown, reactor design parameters are needed. These values are collected in Table 1. Fig. 1 shows the geometric structure of debris relocated in the lower head vessel.

The heat to be removed includes the decay heat released from the radioactive debris and the sensible heat that is contributed as the phase changes from liquid to solid. In case of the TMI-2 accident, specific decay heats were calculated at 224 minutes after shutdown, which corresponds to the time that the major relocation of debris to the lower head occurred, and at 600 minutes for the later cooldown period. The decay heat produced from the selected radionuclide inventory was 0.13 W/g of debris (0.18 W/g of U) at 224 minutes and 0.096 W/g (0.14 W/g of U) of debris at 600 minutes after the accident. Since the debris is rapidly relocated, 50% of the sensible heat is assumed to be released during relocation from the core to the lower plenum. Hence, in order to calculate the heat removal requirement, the sensible heat produced from the phase change must be added to the decay heat produced from the radionuclides.

Since the crust of debris has a poor heat conductivity and the gap between the debris and the RPV wall presents gap heat resistance, 30% of total heat is transferred to the lower head vessel wall. Actually, heat removal requirement consists of 30% decay heat plus 30% sensible heat. Only 50% of total sensible heat is considered to be released within the debris bed in the lower plenum, while the other 50% had already been removed during the relocation process. The sensible heat is calculated from the cooling rate and the specific heat as follows

$$Q_{sensible} = \frac{FMC_p \Delta T}{\Delta t} \tag{8}$$

Heat removal requirements are shown in Figs. 2, 3, 4 and 5 for TMI-2, KORI-2, YGN 3&4 and KNGR, respectively.

3.3. Modeling and Assumptions

To make phase change from the solid to the liquid in a short period of time, the amount of sensible heat greatly contributes to the enthalpy. In the TMI-2 accident, it is reported that the crust was formed over about 2 minutes. Therefore, the sensible heat corresponding to the amount of 19 ton in short period of time is the real removal heat. Though the heat transfer mechanism is complicated, the assumption that will be used in this study is that all the debris becomes a crust. In addition, it is reported that the heat flux generated from the debris dependency on the vessel angle, but it is assumed that there is no heat flux dependency on the vessel angle and that the heat is only removed through the gap between the crust of debris and the RPV wall. At this time, the system pressure is considered to be 10 MPa, and the heat removal through the gap will be dominated by CCFL.

The assumptions made in the current modeling are summarized below :

- Debris is relocated with a pancake crust geometry.
- 30% of the total heat is transferred to the RPV lower head.
- Heat removal requirement consists of decay heat and sensible heat. Heat is only removed through a narrow gap between the debris and the vessel.
- The accident scenario is similar to TMI-2, with the system pressure of 10 MPa.
- Gap cooling is governed by CCFL.

The continuity equation for the two phases in the upper cross section in Fig. 1 becomes

$$\rho_L j_L = \rho_G j_G \tag{9}$$

Maximum heat removal can be calculated from the maximum liquid flow rate through a simple energy balance. The energy balance gives

$$Q_{t,max} = H_{fg} A_G \rho_G j_{G,max} \tag{10}$$

To obtain the superficial velocity of vapor for liquid zero penetration into gap, $j_{G,max}$, equation (5) is applied. Table 2 shows the vapor superficial velocity for four different reactors.

3.4. Maximum Heat Removal Capability

In this study, when the gas superficial velocity is nearly 6 m/s at 10 MPa, CCFL occurs. Results of the analysis show that the heat removal through the gap cooling relative to CCFL was efficacious as much as about 40% of the core material accumulated in the lower plenum. Though there are uncertainties about the assumptions made in the present study, the analyses yield consistent results. If different cooling effects are considered, heat removal may be greatly enhanced. In the TMI-2 accident, approximately nineteen (19) tons (16% of the whole core) of the molten core material drained into the lower plenum. However, the RPV was apparently sustained. The result for TMI-2 proves that the RPV integrity may indeed be saved. Figs. 6, 7, 8 and 9 show the heat removal capability for TMI-2, KORI-2, YGN 3&4 and KNGR, respectively.

4. CONCLUSION

With a number of assumptions introduced, this work has analyzed the maximum heat removal capability through the narrow gap that may be formed during a core melt accident. Some of the assumptions might as well be overly conservative. According to this study, heat removal capability for TMI-2, KOR-2, YGN 3&4 and KNGR was in the range of 30% to 40% of total core mass. If the cooling capability of the intra-derbis pores and crevices is comparable to debris-to-vessel gap heat removal capability, heat removal from the debris will be greatly augmented than heat removal by the gap cooling alone. When the debris is relocated from the core to the lower head, heat removal is required for the sensible heat as well as the decay heat. In the TMI-2 accident, debris relocation was completed in approximately 120 seconds. After several minutes are elapsed, heat removal is required only of the decay heat. As shown in Figs. 2 through 5, the contribution of the sensible heat to heat removal requirement is nearly twice that of decay heat. If the RPV integrity is maintained with gap cooling within short duration (several minutes) of time, it will be sustained with external cooling in a

long-term cooling mode. Since heat removal requirement is only for the decay heat after several minutes, the RPV will not fail with this external cooling.

ACKNOWLEDGMENT

The authors acknowledge the financial support provided for this work by the Korea Electric Power Corporation.

NOMENCLATURE

A_G	annular area in narrow gap
Bo	Bond number
C	constant
C_k	constant
C_p	specific heat
C_w	wall friction factor
D	diameter of tube
F	fraction of total sensible heat
g	gravity constant
H_{fg}	latent heat of evaporation
Ku_G	Kutateladze number of gas phase
Ku_L	Kutateladze number of liquid phase
M	mass of debris
m	constant
m_k	constant
$Q_{sensible}$	sensible heat
$Q_{t,max}$	maximum heat
S	gap size
S*	nondimensional characteristic length
$\Delta T/\Delta t$	cooling rate
ΔT	temperature difference
Δt	time difference
w	average circumference of the annulus

Greek letters

σ	surface tension
j_L^*	nondimensional superficial velocity of liquid phase
j_G^*	nondimensional superficial velocity of gas phase
$j_{G,max}$	superficial velocity of vapor for liquid zero penetration into gap
ρ_G	density of gas
ρ_L	density of liquid

REFERENCES

1. K. Y. SUH, "Modeling of Heat Transfer to Nuclear Steam Supply System Heat Sinks and Application to Severe Accident Sequences," Nuclear Technology, Vol. 106, pp. 274~291, June (1994)
2. K. Y. SUH and R. E. HENRY, "Integral Analysis of Debris Material and Heat Transport in Reactor Vessel Lower Plenum," Nuclear Engineering & Design, Issue Dedicated to Dr. Novak Zuber, Vol. 151, No.1, pp. 203~221, November (1994)
3. K. Y. SUH and R. E. HENRY, "Debris Interactions in Reactor Vessel Lower Plena During a Severe Accident: I. Predictive Model," Nuclear Engineering & Design, Vol. 166, pp. 147~163, October (1996)
4. K. Y. SUH and R. E. HENRY, "Debris Interactions in Reactor Vessel Lower Plena During a Severe Accident: II. Integral Analysis," Nuclear Engineering & Design, Vol. 166, pp. 165~178, October (1996)
5. K. Y. SUH et al., "Melt Coolability Study Within Hemispherical Vessel Lower Plenum," Submitted for Publication in Nuclear Engineering & Design, June (1998)
6. K. Y. SUH, *SONATA-IV*: Simulation Of Naturally Arrested Thermal Attack In Vessel - visualization study using Pyrex belljar and copper hemisphere heater, presented at the Cooperative Severe Accident Research Program (CSARP) Semiannual Review Meeting, Bethesda, MD, USA, May 1-5 (1995)
7. R. E. HENRY et al., "An experimental investigation of possible in-vessel cooling mechanisms," CSARP Meeting, Bethesda, MD, USA, May (1997)
8. Y. MARUYAMA et al., "In-Vessel Debris Coolability Studies in ALPHA Program," Proceedings of the International Topical Meeting on PSA'96, Park City, UT, USA, September (1996)
9. O. L. PUSHKINA and Y. L. SOROKIN, "Breakdown of liquid film motion in vertical tubes," Heat Transfer Sov. Res. 1, pp. 56~64, (1969)
10. G. B. WALLIS, "One dimensional Two-Phase Flow," McGraw-Hill, NY, USA, (1969)
11. H. J. RICHTER, "Flooding in Tubes and Annuli," Int. J. Multiphase Flow, Vol. 7, No. 6, pp. 647~658, (1981)
12. N. ZUBER, "Hydrodynamics aspects of boiling heat transfer," AEC Rep., AECU-4439, June (1959)
13. Y. HARAMURA and Y. KATTO, "A new hydrodynamic model of critical heat flux, applicable widely to both pool and forced convection boiling on submerged bodies in saturated liquids," Int. J. Heat mass Transfer, Vol. 26, No. 3, pp. 389~399 (1983)
14. F. B. CHEUNG and K. H. HADDAD, "A hydrodynamic critical heat flux model for satruated pool boiling on a downward facing saturated pool boiling on a downward facing curved heating surface," Int. J. Heat Mass Transfer, Vol. 40, No. 6, pp. 1291~1302, (1997)

15. J. H. JEONG et al., "Experimental Study on CHF in a Hemispherical Narrow Gap," OECD / CSNI Workshop on In-Vessel Core Retention and Coolability, Garching, Germany, March (1998)
16. L. A. STICKLER et al., "Calculations to estimate the margin to failure in the TMI-2 vessel," NUREG/CR-6196, TMI V(93)EG01, EGG-273, (1994)
17. J. R. WOLF et al., "TMI-2 vessel investigation project integration report," NUREG/CR-6197, TMI V(93)EG10, EGG-2734, (1994)
18. P. HOFMANN et al., "Reactor Core Material Interactions at Very High Temperature," Nuclear Technology, 87, No.1, August (1989)
19. J. K. HOHORST, "SCDAP/RELAP5/MOD2 Code Manual, Volume 4 : MATPRO – A Library of Materials Properties for Light-Water-Reactor Accident Analysis," NUREG/CR-5273, EGG-2555, February (1990)
20. J. L. REMPE et al., "Investigation of the coolability of a continuous mass of relocated debris to a water-filled lower plenum," EG&G Idaho Report, EGG-RAAM-11145, (1994)

Table 1. Design parameters for reactors studied

	TMI-2	KORI-2	YGN 3&4	KNGR
Thermal Power [MWt]	2272	1876	2815	3816
System Pressure [MPa]	15.5	15.5	15.5	15.5
Weight of Assemblies [ton]	127.73	72.9	115.69	157.08
Inner Diameter of Vessel [m]	4.4323	3.35	4.12	4.74

Table 2. Vapor superficial velocity for liquid zero penetration into gap

(Unit : m/s)

	TMI-2	KORI-2	YGN 3&4	KNGR
5%	5.99	4.97	5.50	5.90
10%	6.01	5.02	5.55	5.94
15%	6.04	5.06	5.59	5.98
20%	6.06	5.10	5.63	6.02
25%	6.09	5.14	5.67	6.06
30%	6.11	5.18	5.71	6.09
35%	6.13	5.21	6.74	6.13
40%	6.15	5.25	5.77	6.16
45%	6.17	5.28	5.81	6.19
50%	6.19	5.31	5.84	6.23
55%	6.21	5.33	5.87	6.25
60%	6.22	5.36	5.89	6.28
65%	6.24	5.38	5.92	6.31
70%	6.25	5.40	5.94	6.33
75%	6.26	5.42	5.96	6.36
80%	6.27	5.44	5.98	6.38
85%	6.28	5.45	6.00	6.40
90%	6.29	5.47	6.02	6.42
95%	6.30	5.48	6.04	6.44
100%	6.30	5.48	6.05	6.45

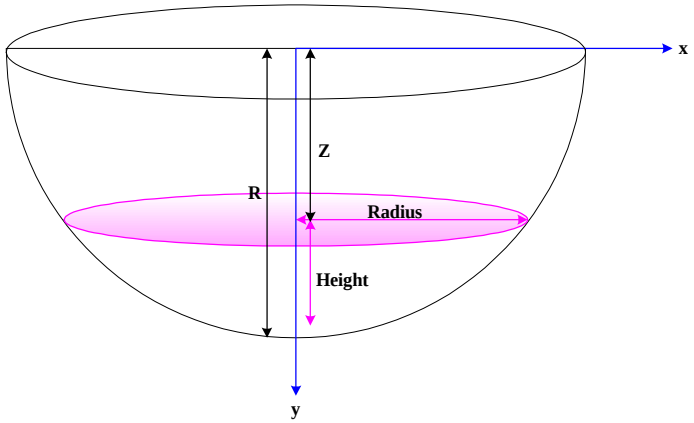

Fig. 1 Hemispherical geometry of debris relocated

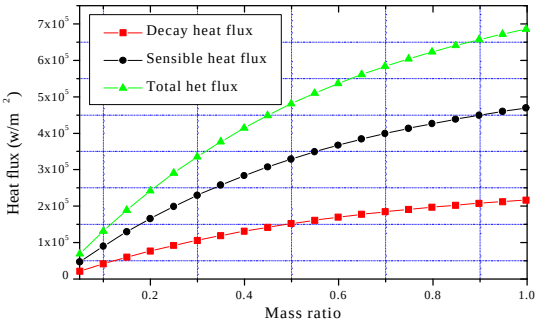

Fig. 2 Heat removal requirement for TMI-2

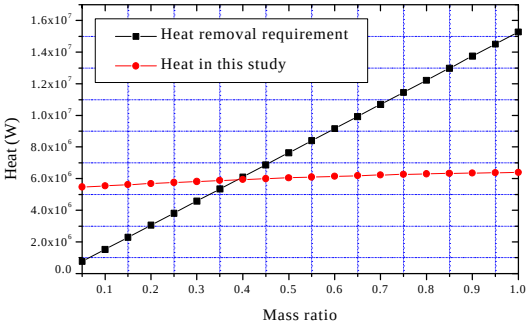

Fig. 6 Maximum heat removal capability in TMI-2

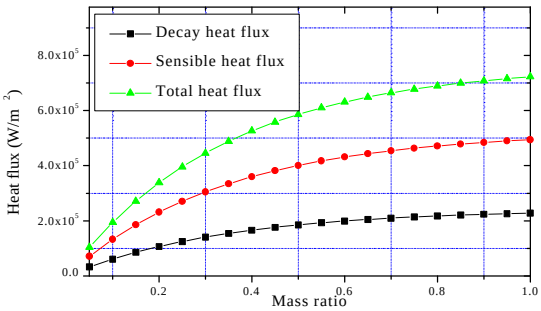

Fig. 3 Heat removal requirement for KORI-2

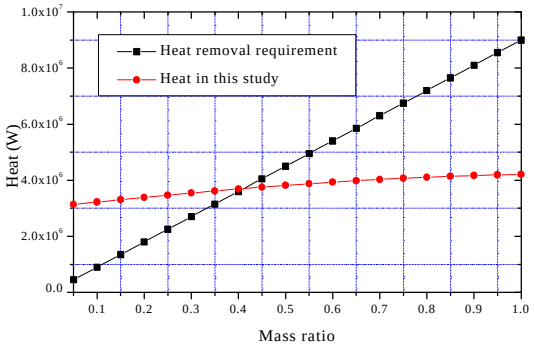

Fig. 7 Maximum heat removal capability in KORI-2

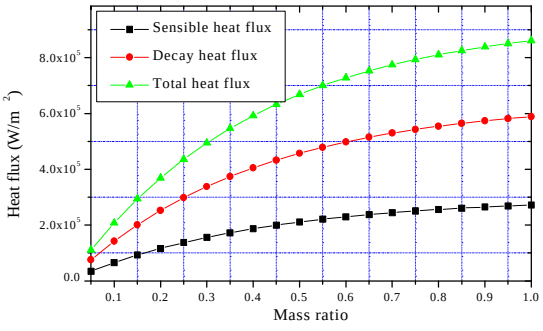

Fig. 4 Heat removal requirement of YGN 3&4

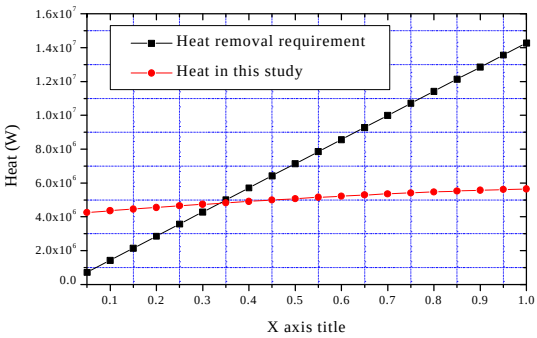

Fig. 8 Maximum heat removal capability in YGN 3&4

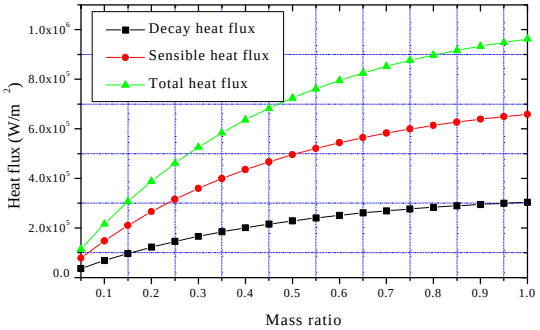

Fig. 5 Heat removal requirement of KNGR

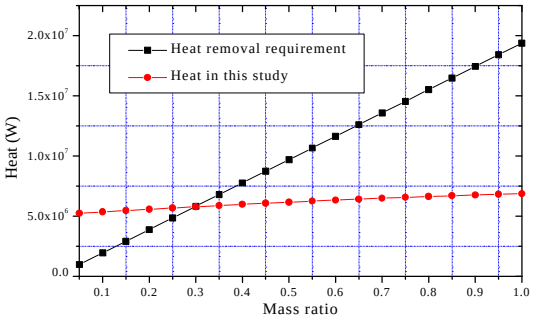

Fig. 9 Maximum heat removal capability in KNGR